

Effect of Bubbling Ar+5% H₂ Gas Mixture on Oxygen Concentration in Static Liquid Lead-Bismuth Eutectic at 350-550°C

Authors: Mr. Xi Kun Wang, Dr. Huiping Zhu, Chang, Prof. Hailong, Prof. Zhenfeng Tong, Chang, Prof. HaiLong

Date: 2024-12-09T19:02:21+00:00

Abstract

Gas-phase oxygen control technology, designed to control the oxygen concentration (Co) in liquid lead-bismuth eutectic (LBE) within an optimal range, represents an effective approach to mitigating corrosion in structural materials. To examine the effects of key parameters including inlet gas flow rate and liquid LBE temperature on the efficiency of this technology, a series of experiments were conducted in static liquid LBE at temperatures ranging from 350-550°C, with an Ar+5%H₂ gas flow of 100-500ml/min. The results were analyzed thermodynamically, to explore comprehensively the oxygen control process. Findings indicate that increases in liquid LBE temperature and inlet gas flow rate markedly enhance the efficiency of oxygen reduction. Specifically, at 550°C, the average oxygen reduction rate achieved 4.35×10^{-5} wt.%/h, which is approximately two orders of magnitude higher than that observed at 350°C (3.11×10^{-7} wt.% reduction are the fundamental factors influencing the deoxygenation limit in liquid LBE, with Fe₃O₄ being the primary determinant.

Full Text

Preamble

Effect of Bubbling Ar+5%H₂ Gas Mixture on Oxygen Concentration in Static Liquid Lead-Bismuth Eutectic at 350–550°C

XiKun Wang,¹ HuiPing Zhu,¹ HaiLong Chang,^{2,3,4,†} and ZhenFeng Tong^{1,‡}

¹North China Electric Power University, Beijing, 102206, China

²Institute of Modern Physics, Chinese Academy of Sciences, Lanzhou, 730000, China

³School of Nuclear Science and Technology, University of Chinese Academy of Sciences, Beijing 100049, China

⁴Advanced Energy Science and Technology Guangdong Laboratory, Huizhou 516000, China

Gas-phase oxygen control technology, designed to regulate the oxygen concentration (C) in liquid lead-bismuth eutectic (LBE) within an optimal range, represents an effective approach for mitigating corrosion in structural materials. To examine the effects of key parameters—including inlet gas flow rate and liquid LBE temperature—on the efficiency of this technology, a series of experiments were conducted in static liquid LBE at temperatures ranging from 350–550°C with an Ar+5%H₂ gas flow of 100–500 ml/min. The results were analyzed thermodynamically to comprehensively explore the oxygen control process. Findings indicate that increases in liquid LBE temperature and inlet gas flow rate markedly enhance the efficiency of oxygen reduction. Specifically, at 550°C, the average oxygen reduction rate achieved 4.35×10^{-5} wt.%/h, which is approximately two orders of magnitude higher than that observed at 350°C (3.11×10^{-7} wt.%/h). Additionally, the average deoxygenation limits (logC) at temperatures of 350°C, 400°C, 450°C, 500°C, and 550°C stabilized at values of -10.33, -9.56, -8.53, -7.98, and -7.70, respectively. The dissolution and precipitation of temperature-dependent oxides that resist H₂ reduction are the fundamental factors influencing the deoxygenation limit in liquid LBE, with Fe₃O₄ being the primary determinant.

Keywords: Liquid lead-bismuth eutectic, Gas-phase oxygen control, Oxygen concentration

Introduction

Liquid lead-bismuth eutectic (LBE) stands out as a prime candidate coolant for lead-based fast reactors (LFRs) as well as for both spallation targets and coolants in accelerator-driven subcritical nuclear systems (ADS). Despite its numerous advantages, such as a high boiling point, low melting point, and excellent thermal conductivity, the corrosion of structural materials remains a major obstacle to the implementation of lead-based nuclear energy systems [?]. Iron-based materials have been the primary choice for structural components in previous studies. The corrosion of these iron-based materials is mainly influenced by the oxygen concentration within the liquid LBE. The oxygen concentration must be precisely controlled to avoid exceeding the threshold for lead oxide formation or falling below the level required to sustain a protective oxide film. The protective oxide layer is essential for mitigating LBE-induced corrosion, thus improving the durability and lifespan of structural materials [?]. Therefore, effective management of the oxygen concentration in liquid LBE is crucial for ensuring the safe and efficient operation of these systems.

Common methods for controlling oxygen concentration in liquid LBE include gas-phase oxygen control, solid-phase oxygen control, and electrochemical oxygen pump technology [?]. Of these, gas-phase oxygen control is the most widely adopted method internationally. This technology regulates oxygen concentra-

tion by directly introducing an inert carrier into the liquid LBE, utilizing hydrogen/oxygen (H_2/O_2) mixtures, or by adjusting the partial pressure of oxygen ($\text{H}_2/\text{H}_2\text{O}$) in the gas above the liquid LBE surface, facilitating equilibrium between the oxides in liquid LBE and the incoming gas. Gas-phase oxygen control is characterized by simple equipment and operation, allowing for effective regulation of oxygen levels [?, ?, ?, ?]. This method is currently employed in large-scale LBE test facilities worldwide, including Belgium's CRAFT, Korea's HELIOS, Germany's CORRIDA, Czech Republic's COLONRI and MATLOO, France's STELLA, Italy's NACIE-UP, LECOR and SHEOPE III, Spain's LINCE, and the United States' DELTA [?, ?, ?].

Research on liquid LBE, especially under gas-phase controlled oxygen environments, primarily focuses on two key areas. First, gas-phase oxygen control methods are widely utilized internationally to establish low oxygen concentrations ($\log C$ between -5 to -7) in liquid LBE at temperatures of 400 to 550°C, primarily for material corrosion and oxygen sensor experiments [?, ?, ?, ?, ?]. Second, despite its widespread application for reducing oxygen concentrations in liquid LBE, research on the effects of gas-phase oxygen control remains limited and primarily addresses the following aspects. Hyo On Nam et al. [?] employed the $\text{Ar} + 4\%\text{H}_2$ bubbling method in the HELIOS loop to reduce oxygen concentration. Their results indicated that the bubbling method, with its larger gas-liquid contact area, offers higher oxygen reduction efficiency than the covering gas method. Carsten Schroer et al. [?] investigated the use of a humidified $\text{Ar} + 5\%\text{H}_2$ mixture to create varying $\text{H}_2/\text{H}_2\text{O}$ ratios, subsequently analyzing and fitting a gas-liquid oxygen transfer model for the covering gas method under gas-phase oxygen control. Kris Rosseel et al. [?] developed a stirrer mechanism to break up LBE bubbles into smaller particles, thereby increasing the gas-liquid contact area and enhancing the oxygen reduction rate. J.L. Courouau et al. [?] conducted experiments on gas-phase oxygen control and concluded that using a ternary gas mixture ($\text{Ar} + \text{H}_2/\text{H}_2\text{O}$) for oxygen reduction, in comparison to a binary mixture ($\text{Ar} + \text{H}_2$), exacerbated LBE contamination.

In summary, various research institutions primarily utilized gas-phase oxygen control to regulate oxygen concentration in liquid LBE systems, which facilitated experiments on material corrosion and sensor calibration. However, relatively few studies have focused on the gas-phase oxygen control process itself, especially regarding its efficiency and mechanisms. Most of the research that was conducted concentrated on enhancing efficiency by increasing the gas-liquid contact surface. Despite this progress, key factors such as liquid LBE temperature and inlet gas flow rate remain underexplored in the literature. The influence of these parameters has not yet been systematically documented. To achieve more effective and precise control of oxygen concentration in liquid LBE systems, it is essential to investigate how these factors influence the gas-phase oxygen control process. This study aims to address these gaps and contribute to a deeper understanding of oxygen management in liquid LBE systems.

This study systematically investigated the effects of liquid LBE temperature

and inlet gas flow rate on the deoxygenation process in gas-phase oxygen control systems. Experiments using the Ar + 5% H_2 bubbling method were conducted over a temperature range of 350°C to 550°C with varying inlet gas flow rates. The effects of these parameters on gas-phase deoxygenation efficiency and oxygen reduction limits were investigated. The resulting data were analyzed to quantify the relationship among liquid LBE temperature, gas flow rate, and deoxygenation performance. This study provides new insights into optimizing oxygen control in liquid LBE systems.

Experimental Setup and Methods

2.1. Oxygen Control Equipment

The oxygen control equipment consists of three primary components: a liquid LBE vessel, an oxygen concentration detection system, and an oxygen control system, as depicted in Fig. 1 [Figure 1: see original paper]. The liquid LBE vessel has an inner diameter of 115 mm and a height of 240 mm, with a liquid LBE height of 100 mm, resulting in a mass of approximately 10.4 kg (43.8% Pb and 56.1% Bi). This vessel is equipped with a gas inlet, gas outlet, temperature probe, and a secure sealing system. A fixed position is provided for the installation of the oxygen sensor within the vessel.

The oxygen control system is composed of gas cylinders, a mixing tank, pipelines, and a detection and control unit. The gas cylinders store argon (Ar), hydrogen (H_2), and oxygen (O_2), each with a purity of 99.999%. The flow of gases from the cylinders into the mixing tank is regulated by flow meters and valves. After mixing, the gas flow into the liquid LBE vessel is controlled by an additional flow meter to ensure uniform distribution. This configuration enables precise regulation of oxygen concentration, which is essential for ensuring the integrity of the experiment. The LBE vessel, shown in Fig. 1, is constructed from 316L stainless steel, and its elemental composition is listed in Table 1.

Over the past year, the LBE in the vessel was subjected to repeated oxygen cycling experiments, leading to fluctuations in oxygen concentration between saturated and undersaturated states. Given the prolonged duration of these experiments, it is reasonable to conclude that the dissolved elements and oxides in the liquid LBE have reached saturation.

Table 1. Chemical composition in wt.% of the austenitic steel 316L.

Element	Si	Cr	Ni	Mo	Fe
Content (wt.%)	0.03	16	11	3	Bal

2.2. Oxygen Sensor

In this experiment, an oxygen sensor independently developed by the Institute of Modern Physics, Chinese Academy of Sciences, was used, as shown in Fig. 2

[Figure 2: see original paper]. The sensor uses a Bi/Bi₂O₃ reference electrode, with molybdenum wire as the lead material, and a solid electrolyte composed of yttrium oxide-doped partially stabilized zirconia (YPSZ). The oxygen sensor operates on the principle of an electrochemical cell, where oxygen ions diffuse from the high-concentration side through oxygen ion vacancies in the solid electrolyte to the low-concentration side. The oxygen concentration in the liquid LBE is determined by the potential difference between the reference and working electrodes, which arises from variations in oxygen concentration. The sensor operates effectively within a temperature range of 280 to 650°C, as reported in previous studies [?, ?]. In our experiments, the sensor exhibited a maximum error of 3% under liquid LBE with saturated oxygen. Notably, at temperatures above 350°C, the error decreased to less than 1%. The internal resistance of the multimeter used for measuring the sensor's potential signal was 1 GΩ.

The electrochemical potential of the sensor is presented below:

Mo, Bi+Bi₂O₃//YPSZ//LBE, 316L

The relationship between the sensor potential and the oxygen concentration in the LBE system can be derived using the Nernst equation, as presented in Equation (1) [?]:

$$\log C_o(\text{wt.}\%) = 2.1715 - \frac{T(K) - 10.08}{E(\text{mV})} \cdot T(K)$$

Table 2. Details of the experimental parameters.

Parameters	Values
Experimental temperature (°C)	350, 400, 450, 500, 550
Gas flow rate (ml/min)	100, 200, 300, 400, 500
Bi ₂ O ₃ sensor temperature range	280 to 650
Bi ₂ O ₃ sensor accuracy	>350°C
Initial oxygen concentration at 350°C (logC)	-
Initial oxygen concentration at 400°C (logC)	-
Initial oxygen concentration at 450°C (logC)	-
Initial oxygen concentration at 500°C (logC)	-
Initial oxygen concentration at 550°C (logC)	-
Resistance acquisition (GΩ)	1
Data acquisition time (s)	-
Mass of LBE (kg)	10.4

2.3. Experimental Parameters

The oxygen control experiment was conducted using the setup shown in Fig. 1. A bubbling oxygen reduction test was performed on 10.4 kg of LBE under an atmosphere of Ar + 5%H₂. The gas-phase oxygen control experiments

were designed with gas flow rates of 100, 200, 300, 400, and 500 mL/min at temperatures of 350°C, 400°C, 450°C, 500°C, and 550°C, respectively.

When the oxygen concentration in the liquid LBE reaches saturation or supersaturation, the oxygen sensor's measured potential corresponds to the saturation level at the respective temperature. However, the sensor potential signal does not indicate the degree of supersaturation in the liquid LBE. To accurately analyze the influence of liquid LBE temperature and gas flow rate on oxygen control, the initial oxygen concentration at each temperature was intentionally maintained below the saturation level. Specific values for the initial oxygen concentrations at various temperatures are listed in Table 2. The saturated oxygen concentration in liquid LBE is determined based on Schroer et al. [?], with the applicable liquid LBE temperature range below 800°C:

$$\log C_o(\text{wt.}\%) = 2.62 - \frac{T(k)}{\dots}$$

In the oxygen reduction experiments conducted at various liquid LBE temperatures and inlet gas flow rates, the oxygen concentration limit is defined as the point at which the oxygen concentration ($\log C$) decreases to a specific value and fluctuates by less than 5%, remaining stable for at least 5 hours.

Table 2 presents the specific experimental parameters. The oxygen reduction data at different liquid LBE temperatures and inlet gas flow rates were analyzed to evaluate their effects on the oxygen reduction process.

Results and Discussion

3.1.1. Oxygen Control Results

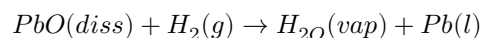
The variation of oxygen concentration in the liquid LBE with different inlet gas flow rates at various liquid LBE temperatures is presented in Fig. 3 [Figure 3: see original paper]. The oxygen reduction limits were observed at each liquid LBE temperature. Obviously, these limits were largely unaffected by the inlet gas flow rates. For example, the oxygen reduction limits ($\log C$) at 400°C for inlet flow rates ranging from 100 to 500 ml/min were -9.55, -9.60, -9.40, -9.60, and -9.63. These limits were mainly influenced by liquid LBE temperature, with the average oxygen reduction limits ($\log C$) ranging from -7.7 at 550°C to -10.33 at 350°C.

The oxygen reduction rate for each condition was calculated by dividing the change in oxygen concentration (from its initial to the limit concentration) by the corresponding deoxygenation time. The oxygen reduction rate increased with higher inlet gas flow rates. This effect became more pronounced at elevated liquid LBE temperatures. In contrast, at 350°C and 400°C, the oxygen reduction curves with different inlet gas flow rates showed negligible variation, suggesting that inlet gas flow rate had limited influence at low temperatures. The detailed experimental results are presented in Table 3 .

Based on the oxygen reduction data in Fig. 3, the trends of deoxygenation with different liquid LBE temperatures and inlet gas flow rates were similar. Initially, the oxygen concentration decreased slowly. As the oxygen concentration decreased further, the deoxygenation rate accelerated, exhibiting a nearly linear downward trend. Finally, the deoxygenation rate slowed again as it approached the oxygen decomposition limit. According to the principles of gas-phase oxygen control, the variation in oxygen reduction rate is closely linked to the reaction sequence of oxides involved in the H_2 reduction process in liquid LBE at different oxygen concentration levels and temperatures.

3.1.2. Oxide Reaction Behavior in Oxygen Control Process

The gas-phase oxygen control process is influenced by the sequence of reactions with oxides involved in liquid LBE. The formation and degradation of these oxides strongly depend on temperature. The deoxygenation reaction relevant to gas-phase oxygen control is expressed in Equation (3):



If the gas-phase oxygen control process strictly follows the reaction outlined in Eq (3), the oxygen concentration would decrease uniformly, with no lower limit for oxygen reduction. However, this expectation contradicted the experimental results in this study, which indicated that the reactions during the oxygen control process were more complex than Eq (3) suggests [?]. The dissolution of most metal elements into liquid LBE suggests that gas-phase oxygen control may be significantly influenced by the presence of various metal oxides.

The liquid LBE vessel is made of 316L stainless steel, which mainly contains Fe, Cr, Ni, Mn, Mo, and Si, all of which can form oxides. The Gibbs free energy for the reaction of these elements with 1 mol of PbO was analyzed using HSC9 software [?]. For specific reactions, such as the formation of $NiCr_2O_4$ from Ni and Cr_2O_3 , and $NiFe_2O_4$ from Ni and Fe_3O_4 , the Gibbs free energy values were obtained from Bassini et al. [?]. The analysis further indicates that oxides such as NiO, Fe_3O_4 , FeO, Mn_3O_4 , Cr_2O_3 , SiO_2 , and MoO_2 may form in liquid LBE, as shown in Fig. 4 [Figure 4: see original paper]. Fig. 4(b) also highlights the potential formation of complex oxides, such as $NiFe_2O_4$, $SiNi_2O_4$, $MnFe_2O_4$, $FeCr_2O_4$, $SiMn_2O_4$, and $NiCr_2O_4$.

As shown in Fig. 4, the activity of these elements above the red hydrogen oxidation reaction is lower than H_2 , suggesting that their corresponding oxides can be reduced by H_2 . Relevant oxides include NiO, $SiNi_2O_4$, $NiFe_2O_4$, and $NiCr_2O_4$. Consequently, in gas-phase oxygen control, the primary oxides reduced by H_2 are PbO, NiO, $SiNi_2O_4$, $NiFe_2O_4$, and $NiCr_2O_4$. Based on Bassini's [?] derivation of the minimum oxygen concentrations for $NiFe_2O_4$ and $NiCr_2O_4$ formation, the minimum oxygen concentrations of the above oxides were correlated with the oxygen reduction curve at 350°C, as depicted in Fig. 5 [Figure 5: see original paper].

In the first stage, all oxides reacted with H_2 , resulting in a slower oxygen reduction rate at saturated oxygen levels. The next stage mainly involved the reduction of nickel and nickel-based complex oxides, as their Gibbs free energy for H_2 reduction was relatively low. This stage was characterized by a faster oxygen reduction rate. Fluctuations during this phase likely resulted from the reaction dynamics of nickel oxides. Stages three to five focused on the reduction of complex nickel oxides. After the fifth stage, Ni-containing oxides in liquid LBE were completely reduced by H_2 . The slowest oxygen reduction rate from stage five to the reduction limit was attributed to oxides most resistant to H_2 reduction. The type and concentration of oxides involved at different stages are the primary factors affecting the oxygen reduction rate.

3.2. Factors Related to Oxygen Control Efficiency

The oxygen reduction curve in Fig. 3 shows that both increasing the liquid LBE temperature and the inlet gas flow rate significantly enhance the oxygen reduction rate. However, their effects differ in magnitude. The following section presents a detailed analysis of how liquid LBE temperature and inlet gas flow rate affect oxygen reduction efficiency.

3.2.1. Gas Flow Rate The inlet gas flow rate plays a critical role in gas-phase oxygen control. Fig. 6 [Figure 6: see original paper] shows the oxygen reduction rates at different inlet gas flow rates under constant liquid LBE temperature conditions. Although the oxygen reduction rate at certain inlet gas flows was lower than in the previous stage, the overall trend showed an increase in oxygen reduction rate with enhanced inlet gas flow. At 550°C , the oxygen reduction rate increased by 234.36×10^{-7} wt.%/h as the inlet gas flow increased from 100 mL/min to 500 mL/min. Similarly, increases of 38.36, 44.36, 10.24, and 2.79×10^{-7} wt.%/h were observed at 500°C , 450°C , 400°C , and 350°C , respectively.

As the liquid LBE temperature decreased, the effect of increasing the inlet gas flow rate on oxygen reduction efficiency diminished. For example, at 350°C and 400°C , every 100 ml/min increase in inlet gas flow rate only increased the oxygen reduction rate by an average of 0.70 and 2.56×10^{-7} wt.%/h, respectively.

The effect of inlet gas flow rate on the oxygen reduction rate is investigated during the gas-phase oxygen control process. Fig. 7 [Figure 7: see original paper] shows the mechanism of the gas-phase oxygen control process, where H_2 from bursting bubbles or permeating from the bubble wall reacts with oxides in liquid LBE. Therefore, the oxygen reduction process primarily occurs at the bubble interface and the surface of the liquid LBE. Moreover, the movement of gas bubbles induces turbidity and fluctuations in the liquid LBE. Variations in inlet gas flow primarily affect the form and dynamics of bubbles in the liquid LBE, without altering the physicochemical properties of the LBE itself. As the inlet gas flow rate increases, both the number and velocity of bubbles entering the liquid LBE improve, which increases the H_2 content and the contact between

H₂ and liquid LBE, thereby accelerating H₂ reduction reactions. Additionally, the increased bubble velocity intensifies the agitation of the liquid LBE, resulting in a higher diffusion rate of elements within the liquid. As a result, the overall oxygen reduction efficiency improves with increasing inlet gas flow rate.

3.2.2. Liquid LBE Temperature The average rate of deoxygenation from the initial oxygen concentration to the limit across different temperatures is presented in Fig. 8 [Figure 8: see original paper], showing a strong temperature dependence in the deoxygenation rate. As the temperature increased, the average oxygen reduction rate increased significantly. Specifically, the average oxygen reduction rate at 500°C was 66 times greater than that at 350°C, while at 550°C, it was 140 times greater than at 350°C. The increase in temperature significantly improved the efficiency of oxygen removal.

The mechanism of temperature effect on oxygen control efficiency is the underlying reaction in oxide reduction, as described in Section 3.1.2. During gas-phase oxygen control, oxides such as PbO, NiO, SiNi₂O₄, NiFe₂O₄, and NiCr₂O₄ are reduced by H₂. The elevated temperature of liquid LBE decreases the Gibbs free energy of oxides involved in the reduction reactions, making these reactions more thermodynamically favorable. Higher temperatures in liquid LBE also enhance element diffusion, further facilitating the oxygen concentration reduction. The changes in liquid LBE temperature primarily affect the thermodynamic properties of the reaction, while the inlet gas flow rate mainly affects the contact between H₂ and liquid LBE. Consequently, the changes in liquid LBE temperature have a more pronounced effect on oxygen reduction efficiency than changes in inlet gas flow rate.

As shown in Fig. 4, the activity of these elements below the hydrogen oxidation reaction curve denoted by the red line is higher than that of H₂, suggesting that the oxides they form are more resistant to reduction by H₂, including Fe₃O₄, FeO, Mn₃O₄, Cr₂O₃, SiO₂, MoO₂, MnFe₂O₄, FeCr₂O₄, and SiMn₂O₄. In 316L stainless steel, the major elements are Fe, Cr, and Ni, with Fe₃O₄ and Cr₂O₃ detected in LBE experiments. Therefore, only the impact of Fe₃O₄ and Cr₂O₃ dissolution and precipitation on oxygen concentration is analyzed here.

Based on the solubility of Fe₃O₄ and Cr₂O₃, the corresponding oxygen concentrations are determined:

$$\log C_{0,Fe_3O_4} = \log C_{0,Cr_2O_3} = (\log K_{Fe_3O_4} - 3 \log C_{Fe}) = (\log K_{Cr_2O_3} - 2 \log C_{Cr})$$

Where $\log K_{Fe_3O_4}$ and $\log K_{Cr_2O_3}$ represent the solubility products of Fe₃O₄ and Cr₂O₃ in LBE, which were derived from Schroer et al. [?] as shown in Eq (6) and (7). Eq (8) is the solubility product of Fe₃O₄ in LBE obtained by Aerts et al. [?].

$$\log K_{Fe_3O_4} = 10.3123 - \frac{T(K)}{\dots}$$

$$\log K_{Cr_2O_3} = 4.4472 - \frac{T(K)}{\dots}$$

$$\log K_{Fe_3O_4} = 10.5 - \frac{T(K)}{\dots}$$

Fe and Cr solubilities were calculated using the following solubility equations reported by Stéphane Gossé [?], which are valid in the temperature range 127–727°C:

$$\log C_s^{Fe} = 2.00 - \frac{T(K)}{\dots}$$

$$\log C_s^{Cr} = 1.12 - \frac{T(K)}{\dots}$$

Under the experimental conditions, it was assumed that the concentrations of Fe and Cr in liquid LBE reached saturation. At this point, the minimum oxygen concentration influenced by Fe_3O_4 and Cr_2O_3 can be determined. Eq (11) was derived from the data in Eq (6), while Eq (12) was obtained from the data in Eq (8):

$$\log C_{min(0, Fe_3O_4)} = 1.0781 - \frac{T(K)}{\dots}$$

$$\log C_{min(0, Fe_3O_4)} = 1.125 - \frac{T(K)}{\dots}$$

$$\log C_{min(0, Cr_2O_3)} = 0.7357 - \frac{T(K)}{\dots}$$

This explains that at low liquid LBE temperature the oxygen reduction efficiency was little influenced by the inlet gas flow rate, as observed in Section 3.2.1. It concludes that as the temperature of liquid LBE increases, both the reduction reaction and element diffusion are enhanced, accelerating the rate of oxygen reduction.

3.3. Effect on Deoxygenation Limits

In the gas-phase oxygen control experiment, a distinct oxygen reduction limit was observed, as discussed in Section 3.1.1. This deoxygenation limit was significantly influenced by the temperature of liquid LBE. As temperature decreased, the deoxygenation limit decreased correspondingly. The average oxygen reduction limits ($\log C$) from 550°C to 350°C were -7.7, -7.98, -8.53, -9.56, and -10.33, as shown in Fig. 9 [Figure 9: see original paper].

Given the nature of gas-phase oxygen control, the deoxygenation limit is likely primarily affected by oxides that are resistant to reduction by H_2 . The contents of these oxides at different temperatures alter the oxygen concentration in liquid LBE. As shown in Fig. 4, the activity of these elements below the hydrogen oxidation reaction curve denoted by the red line is higher than that of H_2 , suggesting that the oxides they form are more resistant to reduction by H_2 , including Fe_3O_4 , FeO , Mn_3O_4 , Cr_2O_3 , SiO_2 , MoO_2 , $MnFe_2O_4$, $FeCr_2O_4$, and $SiMn_2O_4$. In 316L stainless steel, the major elements are Fe, Cr, and Ni, with Fe_3O_4 and Cr_2O_3 detected in LBE experiments. Therefore, only the impact of Fe_3O_4 and Cr_2O_3 dissolution and precipitation on oxygen concentration is analyzed here.

Based on the solubility of Fe_3O_4 and Cr_2O_3 , the corresponding oxygen concentrations are determined. The minimum oxygen concentrations influenced by Fe_3O_4 , as derived from Eq (11) and (12), are nearly identical. The experimentally observed oxygen reduction limit was slightly higher than the minimum oxygen concentration influenced by Fe_3O_4 and significantly higher than the minimum oxygen concentration determined from Cr_2O_3 dissolution analysis. The slight increase in experimental values compared to those from Fe_3O_4 dissolution can be attributed to other oxides' influence. These results indicate that Fe_3O_4 is the primary factor governing the deoxygenation limit in this experiment. However, if Fe_3O_4 solubility in liquid LBE is not saturated, the deoxygenation limit may be influenced by Cr_2O_3 .

Aerts et al. [?] found that the dissolution of Fe_3O_4 in low-oxygen-concentration liquid LBE significantly influenced the oxygen concentration in LBE. Fe_3O_4 is not easily reduced by H_2 , making its removal during the oxygen reduction process difficult, as shown in Fig. 4. Consequently, when the concentration of Fe_3O_4 in LBE reaches saturation, the deoxygenation limit stabilizes at the minimum oxygen concentration determined by the dissolution of Fe_3O_4 .

Conclusions

This study discussed gas-phase oxygen control conducted in a static liquid LBE system at temperatures ranging from 350°C to 550°C, with an Ar + 5% H_2 inlet gas flow rate ranging from 100 to 500 mL/min. Regarding the effects of liquid LBE temperature and inlet gas flow rate on the oxygen control process, several key conclusions follow:

1. The gas-phase oxygen control process in LBE primarily involves the reaction of H_2 with oxides in the system, specifically PbO , NiO , $SiNi_2O_4$, $NiFe_2O_4$, and $NiCr_2O_4$.
2. Increasing the inlet gas flow rate significantly enhances deoxygenation efficiency. At $550^\circ C$, the specific oxygen reduction rate increased by 234.36×10^{-7} wt.%/h when the inlet gas flow increased from 100 mL/min to 500 mL/min. However, the inlet gas flow rate has a negligible effect on the deoxygenation limit. A higher flow rate increases the contact between H_2 bubbles and LBE, improving LBE mixing and thus accelerating deoxygenation efficiency.
3. The increase in liquid LBE temperature strongly improves deoxygenation efficiency. The average oxygen reduction rate at $550^\circ C$ is 140 times higher than that at $350^\circ C$. Elevated temperature promotes reduction reactions between oxides in liquid LBE and H_2 , and accelerates the diffusion of elements, thus improving overall deoxygenation performance.
4. The deoxygenation limit is primarily influenced by the LBE temperature and it decreases as the temperature decreases. At temperatures of $350^\circ C$, $400^\circ C$, $450^\circ C$, $500^\circ C$, and $550^\circ C$, the mean deoxygenation limits logC are observed to decrease progressively from -10.33, -9.56, -8.53, -7.98, to -7.70. The limit is influenced by the solubility and precipitation of impurity oxides in liquid LBE. Notably, the deoxygenation limit is significantly affected by Fe_3O_4 when the content of Fe_3O_4 in LBE reaches saturation.

References

- [1] C. Fazio, V.P. Sobolev, A. Aerts et al., *Handbook on lead-bismuth eutectic alloy and lead properties, materials compatibility, thermal-hydraulics and technologies-2015 edn.* (Organisation for Economic Co-Operation and Development, Paris, 2015), pp. 185–200.
- [2] L. Zhang, Y.W. Yang, Y.C. Gao., Preliminary physics study of the Lead–Bismuth Eutectic spallation target for China Initiative Accelerator-Driven System. *NUCL SCI TECH* 27, 120 (2016). <https://doi.org/10.1007/s41365-016-0114-6>
- [3] L. Gu, X. Su., Latest research progress for LBE coolant reactor of China initiative accelerator driven system project. *Front. Energy.* 15, 810–831 (2021). <https://doi:10.1007/s11708-...>
- [4] W.P. Deng, T. Wan, W.F. Yang et al., Optimization analysis of thermal–hydraulic features of the 2.5 MW LBE spallation target of CiADS. *Ann Nucl Energy.* 196, 110202 (2024). <https://doi.org/10.1016/j.anucene.2023.110202>
- [5] L.F. Yuan, C.L. Wang, Z.P. Liu, Numerical study of lead-bismuth thermal-hydraulic system characteristics under moving conditions. *Ann Nucl Energy.* 196, 110224 (2024). <https://doi.org/10.1016/j.anucene.2023.110224>

- [6] S.J. Yan, H.W. Fang, P.F. Wang et al., Modeling and control strategy of the China accelerator driven sub-critical reactor. *Prog Nucl Energy*. 71, 179-187 (2014). <https://doi.org/10.1016/j.pnucene.2013.11.010>
- [7] W.P. Feng, C. Qin, K.F. Zhang et al., Preliminary study of oxygen mass transfer in the primary circuit of lead cooled fast reactor. *Ann Nucl Energy*. 181, 109536 (2023). <https://doi.org/10.1016/j.anucene.2022.109536>
- [8] Z.J. Deng, S.B. Cheng, H. Cheng., Experimental investigation on pressure-buildup characteristics of a water lump immersed in a molten lead pool. *NUCL SCI TECH*. 34, 35 (2023). <https://doi.org/10.1007/s41365-023-01188-1>
- [9] L.F. Mao, T.Q. Dang, L.Y. Pan et al., Preliminary analysis of polonium-210 contamination for China LEAd-based Research Reactor. *Prog Nucl Energy*. 70, 39-42 (2014). <https://doi.org/10.1016/j.pnucene.2013.07.009>
- [10] W.L. Huang, D.N. Zhou, Experimental study of LBE and water interface thermal-hydraulic behaviour. *Prog Nucl Energy*. 99, 1-10 (2017). <https://doi.org/10.1016/j.pnucene.2017.04.005>
- [11] L. Zhang, Y.W. Yang, Y.C. Gao., Preliminary physics study of the Lead–Bismuth Eutectic spallation target for China Initiative Accelerator-Driven System. *NUCL SCI TECH*. 27, 120 (2016). <https://doi.org/10.1007/s41365-016-0114-6>
- [12] H.Y. Meng, Y.W. Yang, Z.L. Zhao et al., Physical studies of accelerator-driven minor actinide transmutation in the subcritical system. *NUCL SCI TECH*. 30, 91 (2019). <https://doi.org/10.1007/s41365-019-0623-1>
- [13] J.S. Zhang, N. Ling, Y.T. Chen., Oxygen Control Technique in Molten Lead and Lead-Bismuth Eutectic Systems. *NUCL SCI ENG*. 154, 2, 223-232 (2006). <https://doi.org/10.13182/NSE06-A2628>
- [14] C. Schroer, A. Skrypnik, O. Wedemeyer et al., Oxidation and dissolution of iron in flowing lead-bismuth eutectic. *Corros. Sci*. 61, 63-71 (2012). <https://doi.org/10.1016/j.corsci.2012.04.022>
- [15] C. Schroer, O. Wedemeyer, J. Novotny et al., Performance of 9% Cr steels in flowing lead-bismuth eutectic at 450 and 550°C and 10 $\times 10^{-6}$ wt.% dissolved oxygen. *Nucl Eng Des*. 280, 661-672 (2014). <https://doi.org/10.1016/j.nucengdes.2014.01.023>
- [16] L. Martinelli, C. Jean-Louis, B.C. Fanny., Oxidation of steels in liquid lead bismuth: Oxygen control to achieve efficient corrosion protection. *Nucl Eng Des*. 241(5), 1288-1294 (2011). <https://doi.org/10.1016/j.nucengdes.2010.07.039>
- [17] V.S. Rao, J. Lim, I.L.S. Hwang., Analysis of 316L stainless steel pipe of lead–bismuth eutectic cooled thermal-hydraulic loop. *Ann Nucl Energy*. 48, 40-44 (2012). <https://doi.org/10.1016/j.anucene.2012.05.009>
- [18] J.S. Zhang., Oxygen control technology in applications of liquid lead and lead–bismuth systems for mitigating materials corrosion. *J Appl Electrochem*.

43, 755–771 (2013). <https://doi.org/10.1007/s10800-013-0568-8>

[19] Y.F. Wang, X.B. Li, R.X. Liang et al., Simulation of a solid-phase oxygen control system for lead-bismuth eutectic. *Nucl Eng Des.* 394, 111821 (2022). <https://doi.org/10.1016/j.nucengdes.2022.111821>

[20] X. Zeng, Q. Wang, X. Meng et al., Oxygen concentration measurement and control in small static lead-bismuth eutectic experimental facility. *J NUCL TECHNOL.* 57(5), 590–598 (2019). <https://doi.org/10.1080/00223131.2019.1700842>

[21] X.B. Li, R.X. Liang, Y.F. Wang et al., An optimized numerical method for pre-researching non-isothermal liquid LBE oxygen control performance by solid-phase electrochemical lead–bismuth eutectic loop. *NUCL SCI TECH.* 33, 31 (2022). <https://doi.org/10.1007/s41365-022-01023-z>

[22] J. Lim, G. Manfredi, S. Gavrilov., Control of dissolved oxygen in liquid LBE by active oxygen pumping. *Sensor Actuat B-Chem.* 204, 388-392 (2014). <https://doi.org/10.1016/j.snb.2014.07.117>

[23] R.X. Liang, H.P. Zhu, Z.H. Sheng et al., Experimental studies on solid oxygen control performance of lead–bismuth eutectic heat exchanger loop. *Ann Nucl Energy.* 192, 109977 (2023). <https://doi.org/10.1016/j.anucene.2023.109977>

[24] C.L. Wang, Y. Zhang, D.L. Zhang et al., Numerical study of oxygen transport characteristics in lead-bismuth eutectic for gas-phase oxygen control. *NUCL ENG TECHNOL.* 53(7), 2221-2228 (2021). <https://doi.org/10.1016/j.net.2021.01.031>

[25] Y. Zhang, F.L. Zhang, C.L. Wang et al., Oxygen transport analysis in lead-bismuth eutectic coolant for solid-phase oxygen control. *Ann Nucl Energy.* 154, 108128 (2021). <https://doi.org/10.1016/j.anucene.2021.108128>

[26] P.N. Martynov, A.V. Gulevich, Yu.I. Orlov et al., Water-hydrogen technology for heavy liquid metal coolant reduction. *Prog Nucl Energy.* 47, 604-615 (2005). <https://doi.org/10.1016/j.pnucene.2005.05.063>

[27] S. Bassini, A. Antonelli, I. Di Piazza et al., Oxygen control in HLM thermal-hydraulic n-loop facility NACIE-UP. *Prog Nucl Energy.* 105, 137-145 (2018). <https://doi.org/10.1016/j.pnucene.2018.01.006>

[28] A. Aerts, S. Gavrilov, G. Manfredi, Interaction of oxygen–iron alloy in liquid lead-bismuth eutectic. *Phys Chem Chem Phys.* 18, 19526-19530 (2016). <https://doi.org/10.1039/C6CP01561A>

[29] H.O. Nam, J. Lim, D.Y. Han et al., Dissolved oxygen control and monitoring implementation in the liquid lead-bismuth eutectic loop: HELIOS. *J. Nucl. Mater.* 376, 381-385 (2008). <https://doi.org/10.1016/j.jnucmat.2008.02.038>

[30] C. Schroer, O. Wedemeyer, J. Konys., Gas/liquid oxygen-transfer to flowing lead eutectic. *Nucl Eng Des.* 241, 1310-1318 (2011). <https://doi.org/10.1016/j.nucengdes.2010.06.047>

- [31] L. Brissonneau, F. Beauchamp, O. Morier et al., Oxygen control systems and impurity purification in LBE: Learning from DEMETRA project. *J. Nucl. Mater.* 415, 348-360 (2011). <https://doi.org/10.1016/j.jnucmat.2011.04.040>
- [32] L. Košek, L. Rozumová, A. Hojná et al., Mechanism of localized corrosion issues of austenitic steels posed by flowing lead with 10×10^{-7} wt.% oxygen at 480°C up to 16,000 h. *J. Nucl. Mater.* 572, 154045 (2022). <https://doi.org/10.1016/j.jnucmat.2022.154045>
- [33] C. Foletti, G. Scaddozzo, M. Tarantino et al., ENEA experience in LBE technology. *J. Nucl. Mater.* 356, 264-272 (2006). <https://doi.org/10.1016/j.jnucmat.2006.05.020>
- [34] F.J. Martín-Muñoz, L. Soler-Crespo, D. Gómez-Briceño., Corrosion behaviour of martensitic and austenitic steels in flowing lead-bismuth eutectic. *J. Nucl. Mater.* 416, 87-93 (2011). <https://doi.org/10.1016/j.jnucmat.2011.01.108>
- [35] F. Niu, R. Candalino, N. Li., Effect of oxygen on fouling behavior in lead-bismuth coolant systems. *J. Nucl. Mater.* 366, 216-222 (2007). <https://doi.org/10.1016/j.jnucmat.2007.01.223>
- [36] H. Wang, Q. Yuan, L.J. Chai et al., Effects of pulsed laser surface remelting on microstructure, hardness and lead-bismuth corrosion behavior of a ferrite/martensitic steel. *NUCL ENG TECHNOL.* 54, 6, 1972-1981 (2022). <https://doi.org/10.1016/j.net.2021.12.030>
- [37] H. Li, H.P. Zhu, R.X. Liang et al., Natural circulation transient thermal-hydraulic analysis and corrosion precipitation study in a LBE flow loop. *Nucl Eng Des.* 419, 112975 (2024). <https://doi.org/10.1016/j.nucengdes.2024.112975>
- [38] W.W. Luo, Q.Y. Huang, Y. Luo et al., Effect of minor addition of Ce on microstructure and LBE corrosion resistance for CLAM steel. *Corros. Sci.* 209, 110796 (2022). <https://doi.org/10.1016/j.corsci.2022.110796>
- [39] J. Konys, H. Muscher, Z. Voß et al., Oxygen measurement in stagnant lead-bismuth eutectic using electrochemical sensors. *J. Nucl. Mater.* 335, 249-253 (2004). <https://doi.org/10.1016/j.jnucmat.2004.07.018>
- [40] J.L. Courouau., Electrochemical sensors for on-line monitoring oxygen status in lead-bismuth alloys: development. *J. Nucl. Mater.* 335, 254-259 (2004). <https://doi.org/10.1016/j.jnucmat.2004.07.020>
- [41] A.K. Rivai, T. Kumagai, M. Takahashi., Performance of oxygen sensor in liquid lead-bismuth at low temperature. *Prog Nucl Energ.* 50, 575-581 (2008). <https://doi.org/10.1016/j.pnucene.2007.11.043>
- [42] Y. Zeng, W.F. Fu, X.F. Yu et al., Liquid metal embrittlement and fracture behavior of three Mo metals in liquid lead-bismuth eutectic. *J. Nucl. Mater.* 603, 155434 (2025). <https://doi.org/10.1016/j.jnucmat.2024.155434>
- [43] D. Wang, S.R. Liu, X.F. Ma et al., Enhanced corrosion resistance of austenitic steel 15-15Ti by shot peening processing in liq-

uid lead-bismuth eutectic at 550°C. *Corros. Sci.* 226, 111640 (2024). <https://doi.org/10.1016/j.corsci.2023.111640>

[44] K. Rosseel, J. Lim, A. Marino., HELIOS3: A stirred bubble column for oxygen addition or reduction in lead-bismuth eutectic. *Nucl Eng Des.* 365, 110716 (2020). <https://doi.org/10.1016/j.nucengdes.2020.110716>

[45] J.L. Courouau, P. Trabuc, G. Laplanche et al., Impurities and oxygen control in lead alloys. *J. Nucl. Mater.* 30, 53-59 (2002). [https://doi.org/10.1016/S0022-3115\(01\)00726-7](https://doi.org/10.1016/S0022-3115(01)00726-7)

[46] J. Lim, G. Manfredi, A. Mariën et al., Performance of potentiometric oxygen sensors with LSM-GDC composite electrode in liquid LBE at low temperatures. *Sensor Actuat B-Chem.* 188, 1048-1054 (2013). <https://doi.org/10.1016/j.snb.2013.08.017>

[47] S. Bassini, A. Antonelli, I. Di Piazza et al., Oxygen sensors for Heavy Liquid Metal coolants: Calibration and assessment of the minimum reading temperature. *J. Nucl. Mater.* 486, 197-205 (2017). <https://doi.org/10.1016/j.jnucmat.2017.01.031>

[48] C. Schroer, J. Konys., *Physical Chemistry of Corrosion and Oxygen Control in Liquid Lead and Lead-Bismuth Eutectic*. (Forschungszentrum Karlsruhe, Karlsruhe, 2007), pp. 22-34.

[49] HSC-Chemistry® [Software]. 2021. Roine, A, www.mogroup.com/hsc.

[50] S. Gossé., Thermodynamic assessment of iron, chromium, and nickel solubility and activity in lead bismuth eutectic. *J. Nucl. Mater.* 449, 122-131 (2014). <https://doi.org/10.1016/j.jnucmat.2014.03.011>

Note: Figure translations are in progress. See original paper for figures.

Source: ChinaXiv — Machine translation. Verify with original.